

## Electronic supplementary information

### Connecting structure, dynamics and viscosity in sheared soft colloidal liquids: A medley of anisotropic fluctuations

Fabian Westermeier, David Pennicard, Helmut Hirsemann, Ulrich H. Wagner, Christoph Rau, Heinz Graafsma, Peter Schall, M. Paul Lettinga, and Bernd Struth

#### S1. Viscosity of sample system and PPG 4000

The dependence of the viscosity as a function of shear rate for both, the colloidal sample system as well as of pure PPG 4000 is displayed in figure S1.

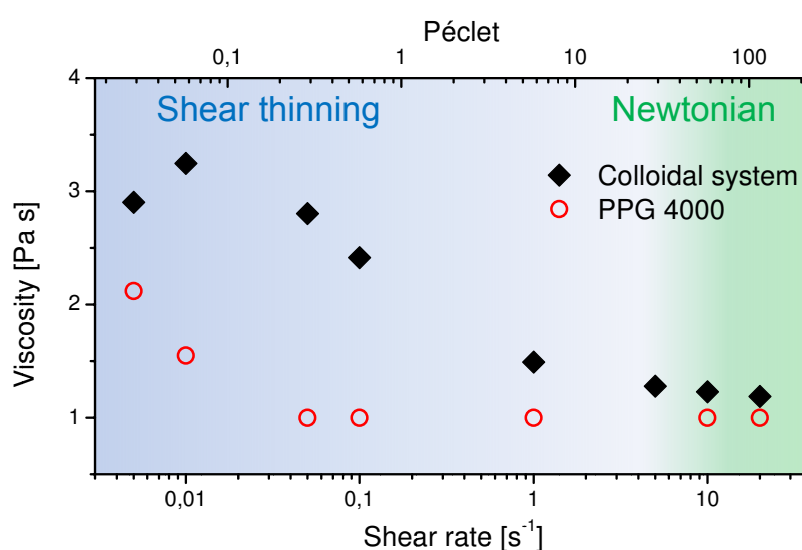


Fig. S1: Viscosity as a function of shear rate for the colloidal sample system and PPG 4000.

While the viscosity of the pure suspension medium PPG 4000 drops at the lowest measured shear rates and is otherwise constant for the measured range of shear rates from  $0.05 - 20 s^{-1}$ , the sample consisting of a suspension of colloidal nanoparticles in PPG 4000 shows a shear thinning behavior in the range of  $\dot{\gamma} = 0.05$  to  $5 s^{-1}$  ( $Pe = 0.25$  to  $25$ ). For even higher shear rates, the viscosity only drops slightly, which indicates the transition from the shear thinning regime to the Newtonian regime.

## S2. Angular dependence of the intensity autocorrelation function

During rheological experiments, X-ray scattering pattern series were recorded with 10000 to 24000 frames per series, covering the start-up, continuous steady-state and cessation of shear in the rheology experiment. From these scattering pattern series, 5000 succeeding images at steady shear conditions were selected and autocorrelation functions were calculated for each pixel individually from the selected patterns. Figure S2 shows such a 2D autocorrelation map for  $Pe = 0.576$  and a delay time  $\tau = 0.008$  seconds.

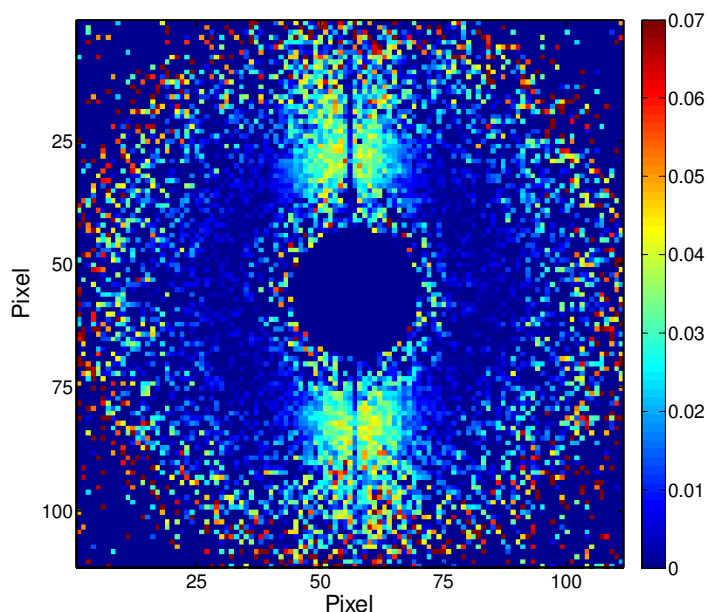


Figure S2: Two-dimensional map of the autocorrelation function  $g_2(\tau = 8 \text{ ms})$  taken at a Péclet number of 0.576. The map is zoomed into the region of interest close to the direct beam. The dark round shape in the middle of the map is a beamstop, covering the region of the direct beam. The vertical streak of lower intensity located in the middle of the map is a result of parasitic slit scattering, showing no correlations (the parasitic slit scattering in the horizontal is removed by crystal optics). The slight tilt of the region of high correlation is a result of a slight mismatch of  $2^\circ$  between flow direction and the horizontal axis of the detector.

The autocorrelation map in figure S2 shows strong anisotropy, revealing the influence of flow on the autocorrelation pattern. The flow direction in figure S2 is horizontally from the left to the right. Perpendicular to this direction a vertical band of strong correlated scattering signal can be identified. In the presence of flow, this band decays slowest compared to the other directions. The width of this vertical band is considerable and thus close to the vertical axis the correlation is relatively insensitive to the flow direction.

The spherical shape of the correlation map is a result of the roughly isotropic scattering intensity distribution  $I(Q)$ , which is decreasing with  $Q$  and thus does not allow for the computation of intensity auto-correlation functions based on single pixels when the scattering intensity per pixel is too low.

To demonstrate the sensitivity to the flow direction, autocorrelation functions were calculated for azimuthal slices of a width of  $10^\circ$ . The azimuthal dependence of the autocorrelation functions in the flow-vorticity plane is depicted in figure S3.

The calculated autocorrelation functions show a strong dependence on the azimuthal angle, decaying fastest in flow direction and slowest perpendicular to this direction.

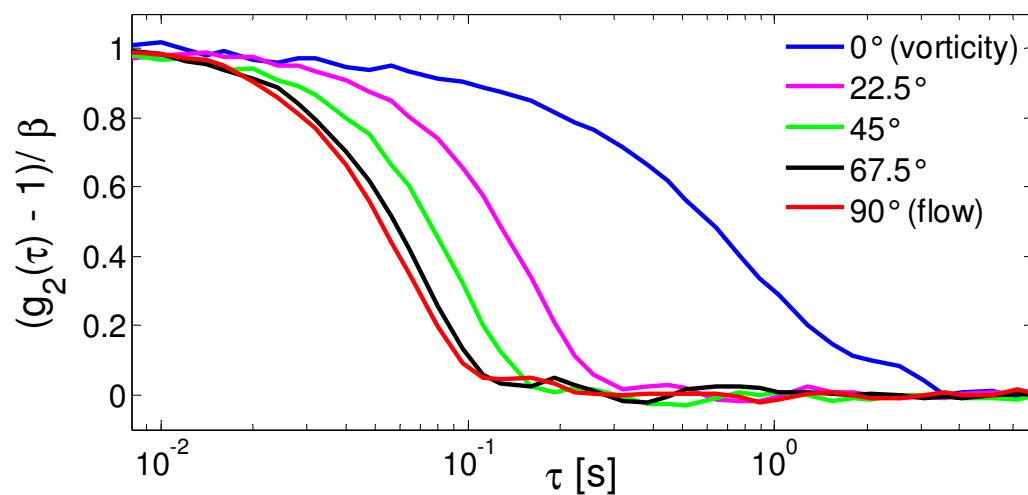


Fig. S3: Azimuthal dependence of the normalized intensity autocorrelation function  $g_2$  calculates in the flow-vorticity plane.